Effect of the reference wave in Auger-electron holography

D. K. Saldin, G. R. Harp,* and B. P. Tonner
Department of Physics and Laboratory for Surface Studies, University of Wisconsin–Milwaukee, 1900 East Kenwood Boulevard, Milwaukee, Wisconsin 53211
(Received 7 November 1991)

We investigate the effect of the angular-momentum character of the emitted wave on Auger electron diffraction patterns, and on the form of holographically reconstructed images of scattering atoms in the vicinity of the emitter. We find that this can have as much effect on the nature of the reconstructed image as the anisotropy of the atomic scattering factors. As in the case of the scattering factors, isotropy of the reference wave is the optimum form for good image reconstruction. We show with both model calculations and experimental Auger electron diffraction data that a reconstruction algorithm which simultaneously corrects for the anisotropy of both source and scatterer is capable of reproducing atom images at their correct positions even in the case of non-*s*-wave emitters.

I. INTRODUCTION

Two recent developments have caused a considerable resurgence of interest in the study of the angular distributions of Auger electrons emitted near a surface and the subsequent multiple scattering by their near-neighbor atoms.

The first is a controversy surrounding experiments by Frank *et al.*[1] in which the conventional view that electron intensities are enhanced in the so-called forward-scattering (or "forward-focusing") directions along chains of scattering atoms was challenged by the suggestion that, instead, intensity dips are found along these directions. To explain their observations, Frank *et al.*[1] proposed an alternative theory in which electrons are assumed to be "blocked" by some form of inelastic scattering mechanism at the scattering atoms. This suggestion has received much criticism[2–5] by others in the field. Recent work by Terminello and Barton[6] appears to have vindicated the experimental observations of Frank *et al.*,[1] but has pointed to some aspect of the initial emitted-electron state in the Auger process to be the cause of the apparently anomalous forward-scattering dips.

The second recent cause of the renewed interest in Auger electron diffraction has been the suggestion by Szöke[7] that an Auger electron diffraction pattern (among others formed from atomic electron sources) may be understood in terms of holographic concepts, thereby pointing toward a means of the direct reconstruction of atomic structures. Using an algorithm due to Barton,[8] Harp, Saldin, and Tonner[12] have holographically reconstructed the positions of the nearest-neighbor atoms to emitter atoms near a Cu(100) single-crystal surface, thus pointing the way to another direct method in crystallography.

In fact, of the many means of implementing atomic-resolution holography with reference waves from atomic sources,[7–12] Auger electron diffraction must be considered one of the most attractive since such diffraction patterns are capable of being generated by relatively inexpensive laboratory equipment, angular distributions from chemically distinct atoms can be measured separately, and the nature of the emitted-electron state, which forms the reference wave in Auger holography, is capable of being calculated by well-established theories.[13,14] In this paper we make a detailed examination of the principles of Auger electron holography.

As in all of the above recently proposed schemes for electron holography, image reconstruction is performed by computer, rather than by the analog method suggested by Gabor, used in most of present-day optical holography. The algorithm proposed by Barton[8] was derived from the Helmholtz-Kirchhoff integral and cast in the form of a phased two-dimensional Fourier transform. The positions of scattering objects are reconstructed well by this algorithm for isotropic reference and scattered waves, but model calculations have shown that, for real atomic scatterers, images of the atoms are found to be somewhat displaced from the true atomic positions.[15–18] These displacements have been attributed mostly to the anisotropic nature of atomic scattering factors for electrons. Consequently, more sophisticated algorithms[15–18] have been suggested for reconstructing more accurately the positions of the atomic scatterers, which are based, in one way or another, on correcting for the anisotropic scattering factors.

We point out in this paper that, as in the explanation of the apparently anomalous results of Frank *et al.*[1] on the form of Auger-electron diffraction patterns, an essential determinant of the nature of a reconstructed holographic image is the form of the reference wave. We illustrate this by simulating Auger electron diffraction patterns from initial states of various angular momentum character, and by examining their effects on the reconstructed images. We compare these simulations with images from measured Auger electron diffraction patterns. We develop a theory for understanding these effects.

We point out that an algorithm which corrects only for the anisotropy of the atomic scattering factor can make reconstructed images worse. The only procedure that

would be expected to work under all circumstances is one which simultaneously corrects for the effect of both the reference and scattered waves. Our algorithm, the scattered-wave-included Fourier transform (SWIFT),[16–18] accomplishes this, as we illustrate with both calculated and measured Auger electron diffraction patterns.

II. THE DIFFRACTION OF AUGER ELECTRONS FROM THEIR ATOMIC NEIGHBORS

Consider an electron source at the origin emitting a spherical wave

$$A_L h_l^{(1)}(kr)Y_L(\hat{\mathbf{k}}) , \tag{1}$$

scattered by an atom at the position $\mathbf{r}_j$. The resulting wave field detected in the far field in a direction specified by $\hat{\mathbf{k}}$ can be written

$$\psi(\mathbf{k})=A_L(i^{-l}Y_L(\hat{\mathbf{k}}) + \sum_{L'} G_{LL'}(k\mathbf{r}_j)t_{l'}e^{-i\mathbf{k}\cdot\mathbf{r}_j}i^{-l'}Y_{L'}(\hat{\mathbf{k}})) . \tag{2}$$

In the above expressions A_L is a complex amplitude, L ($\equiv lm$) and L' ($\equiv l'm'$) represent angular momentum quantum numbers, $h_l^{(1)}$ is a Hankel function of the first kind, Y_L a spherical harmonic, $G_{L',L}$ an element of the free-space propagator in an angular-momentum basis, $\mathbf{k}$ the wave vector of the electrons, $\mathbf{r}$ a position vector, and

$$t_l=ie^{i\delta_l}\sin\delta_l \tag{3}$$

is an element of the atomic t matrix, where δ_l is the phase shift of a spherical wave of angular momentum l on scattering from the atom. In deriving (2) we have made use of the asymptotic expansion of $h_l^{(1)}(z)$ as $z\rightarrow\infty$, namely,

$$h_l^{(1)}(z)\sim i^{-l}e^{iz}/iz , \tag{4}$$

and omitted some common constant factors.

Although the Green's functions $G_{L'L}$ may be evaluated exactly by the formula

$$G_{LL'}(k\mathbf{r})=4\pi\sum_{L''} i^{l-l'-l''}(-1)^{m'-m''}h_{l''}^{(1)}(kr) \times Y_{l'',-m''}(\hat{\mathbf{r}})\int Y_{lm}Y_{l''m''}Y_{l',-m'}d\Omega , \tag{5}$$

as is customary in work on the electronic structure of solids[19,20] or in the study of x-ray-absorption near-edge structure (XANES),[21,22] this turns out to be very time-consuming for electron energies of greater than a few hundred electron volts (eV), which are of interest in the electron holography of atomic structures.[8–12] In order to resolve atomic structures, the electron wavelength should be significantly smaller than the distances between the atoms studied, and this implies that

$$kr\gg 1 . \tag{6}$$

Under such circumstances the Green's function may be approximated by[23]

$$G_{LL'}(kr)=4\pi i^{l'-1}(e^{ikr}/ikr)Y_{L'}^*(\hat{\mathbf{r}})Y_L(\hat{\mathbf{r}}) . \tag{7}$$

This may be regarded as the lowest-order approximation to a "separable" Green's function as defined by Rehr and Albers.[24] Substituting (7) into (2) and dropping the common factor i^{-l}, we can write

$$\psi(\mathbf{k})=A_L[Y_L(\hat{\mathbf{k}}) +(e^{ikr_j}/r_j)Y_L(\mathbf{r}_j)e^{-i\mathbf{k}\cdot\mathbf{r}_j}f(\mathbf{k}\cdot\mathbf{r}_j)] , \tag{8}$$

where

$$f(\mathbf{k}\cdot\mathbf{r}_j)=\frac{1}{ik}\sum_{l'}(2l'+1)t_{l'}P_{l'}(\hat{\mathbf{k}}\cdot\hat{\mathbf{r}}_j) \tag{9}$$

is the "plane-wave" atomic scattering factor,[15] and $P_{l'}$ represents a Legendre polynomial. Systematically more accurate approximations for $\psi(\mathbf{k})$ may be written, using higher-order separable Green's functions[24] and the so-called spherical-wave corrected atomic scattering factors,[26,18] but we will not pursue them in this paper.

It is a common assumption that an Auger electron is equally likely to be emitted in all directions since an Auger transition involves atomic inner-shell processes, and since any memory of the initial excitation process which creates the core hole is assumed to be lost. This implies that

$$A_{lm}\equiv A_l , \tag{10}$$

i.e., that the amplitudes of waves emitted into states of different magnetic quantum numbers m of the same angular momentum quantum number l are equal. It is also assumed that each of these states is excited incoherently with respect to the others. Thus the angular distribution of Auger electrons scattered by the single atom above can be derived from (8) and (10) to be

$$I(\mathbf{k})=\sum_l\frac{2l+1}{4\pi}|A_l|^2\left[1+[f(\hat{\mathbf{k}}\cdot\hat{\mathbf{r}}_j)/r_j]^2+\left[e^{i(\mathbf{k}\cdot\mathbf{r}_j-kr_j)}\sum_m Y_{lm}^*(\hat{\mathbf{k}})Y_{lm}(\hat{\mathbf{r}}_j)[f(\hat{\mathbf{k}}\cdot\hat{\mathbf{r}}_j)/r_j]^*+\text{c.c.}\right]\right] , \tag{11}$$

where we have made use of the relation

$$\sum_m|Y_{lm}(\hat{\mathbf{R}})|^2=\frac{2l+1}{4\pi} , \tag{12}$$

for an arbitrary direction $\hat{\mathbf{R}}$, and c.c. denotes complex conjugate. Notice that the interference term within the large parentheses in (11) can be simplified if we take the direction of the polar axis along that of $\mathbf{r}_j$. Since then

$$Y_{lm}(\hat{\mathbf{r}}_j)=[(2l+1)/4\pi]^{1/2}\delta_{m0}\ , \tag{13}$$

Eq. (11) can be rewritten

$$I(\mathbf{k})=\sum_l \frac{2l+1}{4\pi}|A_l|^2\left[1+[f(\hat{\mathbf{k}}\cdot\hat{\mathbf{r}}_j)/r_j]^2+\{e^{i(k\cdot r_j-kr_j)}P_l(\hat{\mathbf{k}}\cdot\hat{\mathbf{r}}_j)[f(\hat{\mathbf{k}}\cdot\hat{\mathbf{r}}_j)/r_j]^*+\text{c.c.}\}\right]\ , \tag{14}$$

Thus the interference between the emitted and scattered waves may be thought of as occurring only via the spherical waves of magnetic quantum number $m=0$ with the respect to the emitter-scatterer axis. That this is not a result which depends on a particular choice of axis, and that it indeed holds on a single-scattering model even in the presence of many scattering atoms can be seen by noting that alternatively (14) may be derived from (11) by the general relation

$$P_l(\hat{\mathbf{k}}\cdot\hat{\mathbf{r}}_j)=\frac{4\pi}{2l+1}\sum_m Y^*_{lm}(\hat{\mathbf{r}}_j)Y_{lm}(\hat{\mathbf{k}})\ . \tag{15}$$

Since not only this interference term, but also the squared terms within the first set of curly brackets in (14) reflect azimuthal symmetry about the emitter-scatterer axis, so will the diffraction pattern as a whole, despite the fact that the electrons emitted into *individual* mutually incoherent magnetic quantum number channels may not have any such symmetry. One of the consequences of this symmetry of the diffraction pattern is that for many purposes it may be advantageous to *choose* as a polar axis the direction between emitter and scatterer.

III. THE HOLOGRAPHIC RECONSTRUCTION ALGORITHM AS A ONE-DIMENSIONAL FOURIER TRANSFORM

We begin our consideration of Auger electron holography by reconsidering the algorithm

$$A(\mathbf{r})=\int I(\mathbf{k})e^{-ik\hat{\mathbf{k}}\cdot\mathbf{r}}d\hat{\mathbf{k}}$$

$$=\int\int I(\mathbf{k})e^{-ik_z z}e^{-i(k_x x+k_y y)}\frac{1}{\cos\theta}dk_x\,dk_y \tag{16}$$

proposed by Barton[8] for reconstructing an image of the atomic environment near an emitting atom by direct mathematical processing of the angular distribution of a diffraction pattern $I(\mathbf{k})$. In (16), A represents the amplitude of the reconstructed image, $\mathbf{k}=(k_x,k_y,k_z)$ the wave vector of the electron forming the corresponding point on the diffraction pattern, $\mathbf{r}=(x,y,z)$ a position vector in the image space, and θ the polar angle of the vector $\mathbf{k}$ with respect to the z axis. In this expression the Cartesian axes (x,y,z) are fixed relative to the experimental apparatus.

For the general reconstruction of a full three-dimensional image, (16) or its modifications[16–18] represent an efficient way of calculating it. In the spirit of our discussion of the Auger electron diffraction patterns of the previous section, however, it would seem to be profitable to employ a more flexible definition of the coordinate axes. If the directions of atomic rows radiating from emitter atoms can be guessed from the appearance of a diffraction pattern, as has been asserted in the case of so-called "forward-scattering" or "forward-focusing" diffraction patterns, the missing piece of crystallographic data is information concerning the distance of the scattering atom from the emitter. It was originally hoped that this information might be found by plotting a so-called "radial image function" (or RIF, for short)[12] and that the radial distance of this atom from the source would correspond to a peak of the reconstructed intensity along this line. It was subsequently recognized[15–18] that the very nonisotropic nature of the atomic scattering factors, which gives rise to the forward-scattering effect is also the cause of systematic displacements of the image peak on an RIF from the true position of the scattering atom. In an earlier paper[17] we showed that (16) may be reformulated to express the RIF as a one-dimensional Fourier transform of the azimuthally-integrated polar angle variation of the diffraction intensity when the direction of the RIF is taken as that of the polar axis. In this case it is easy to see that the reconstructed intensity along the RIF can be written

$$A(z)=-k^2\int\left[\int I(k,\theta,\phi)d\phi\right]e^{ikz\cos\theta}d(\cos\theta)\ . \tag{17}$$

Defining

$$k_z=k\cos\theta\ , \tag{18}$$

and

$$J(k_z)=\int I(k,\theta,\phi)d\phi\ , \tag{19}$$

(17) may be rewritten as

$$A(z)=-k\int J(k_z)e^{-ik_z z}dk_z\ . \tag{20}$$

Hence we observe that the radial distance z from the emitter, and k_z may be regarded as conjugate variables of a one-dimensional Fourier transform. In the following we will show that the well-known properties of Fourier transforms may be invoked to provide understandings of the role of various features of diffraction patterns in the formation of atomic images on reconstruction.

For Auger electron diffraction from a single source and a single scatterer, as considered in the last section, where the diffraction intensity has azimuthal symmetry about the source-scatterer axis, very interesting *analytic* results follow from the use of Eq. (20), if we *choose* our polar axis (z) to lie along this axis. The absence of any azimuthal dependence of the diffraction intensity enables Eq. (14) to be recast in the simpler form

$$I(\mathbf{k})=I(k_z)=\sum_l \frac{2l+1}{4\pi}|A_l|^2\{1+[f(k_z)/z_j]^2 + \cdots + \{e^{i(k_z z_j - k z_j)}P_l(k_z/k)[f(k_z)/z_j]^* + \text{c.c.}\}\ , \quad (21)$$

i.e., we may regard I as a function of only the magnitude of the z component of the electron wave vector associated with the corresponding point on the diffraction pattern.

The azimuthal integral in (19) then yields just a factor of 2π and the corresponding RIF along the z axis can be evaluated from (20) as

$$A(z)=2\pi k\int_0^{k_{z,\max}} I(k_z)e^{-ik_z z}dk_z\ . \quad (22)$$

In the following sections we will examine the consequences of this integral for a number of special cases.

IV. s-WAVE EMITTER

Expression (21) is considerably simplified if the dominant channel of the emitted waves corresponds to $l=0$ (an s wave). In this case we may write

$$I(k_z)=(|A_0|^2/4\pi)(1+[f(k_z)/z_j]^2 + \{e^{ik_z z_j}e^{-ikz_j}[f(k_z)/z_j]^*+\text{c.c.}\})\ . \quad (23)$$

If, in addition, we consider an s-wave scatterer, the scattering factor reduces to the form,

$$f(k_z)=(1/ik)t_0=f_0e^{i\sigma}\ , \quad (24)$$

say, a complex quantity with neither angular nor position dependence (we take f_0 and σ as real). Then (23) simplifies further to

$$I(k_z)=(|A_0|^2/4\pi)\{1+[f_0/z_j]^2 + 2[f_0/z_j]\cos[(k-k_z)z_j+\sigma]\}\ . \quad (25)$$

A plot of $I(k_z)$ versus k_z would thus be of pure sinusoidal character, as shown by the dashed line in Fig. 1. The curve shown was calculated from (25) for $k=8.2$ (a.u.)$^{-1}$ (corresponding to an electron energy of 914 eV) and taking $z_j=4.8$ a.u. (=2.54 Å, the spacing of nearest-neighbor atoms in a Cu crystal), and $\sigma=0$. If the range of k_z were infinite, of course the Fourier transform of (22) would yield just three δ functions at $z=\pm z_j$ and $z=0$. The origin of the $\pm$ pair can be most clearly seen by decomposing the cosine term in (25) into its two complex exponential components. The δ function at $z=0$ is due to the constant terms preceding the cosine in (25). This may be removed by subtracting the mean value of $I(k_z)$ *prior* to Fourier transforming. In practice, of course, diffraction data can only be measured over a finite range of k_z. If source and scatterer were aligned perpendicular to a surface, since an electron diffraction pattern may be detected only over a hemisphere covering the half-space outside the surface, k_z would at best range from 0 to k. In practice, detection of electrons emerging close to a glancing angle to the surface is difficult, and more typically measurement of a diffraction pattern is restricted to polar angles with respect to the surface normal in the range 0° to about 70°. Assuming a maximum polar angle of 70°, k_z/k would range from 0.34 to 1, as depicted in Fig. 1. Thus in practice $I(k_z)$ can be thought of as a cosine wave multiplied by a top-hat function spanning just the measurable range of k_z. From the convolution theorem, the Fourier transform of this product is the convolution of the Fourier transforms of the factor functions: i.e., the convolution of the δ functions with a sinc function whose width is inversely proportional to the k_z range. Thus the resulting RIF would consist of sinc functions centered around the precise position of the scatterer and its twin.[18,17] In the absence of significant overlap of the sinc functions, the resulting intensity RIF is independent of the constant phase σ.

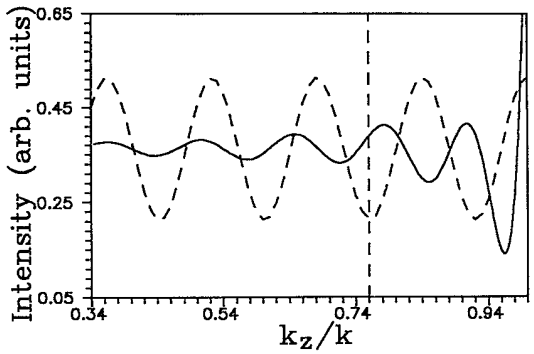

FIG. 1. Far-field diffraction intensity (solid line) of a Cu atom scatterer 2.54 Å along the z axis from an s-wave source of 914-eV electrons as a function of the normalized z component, k_z/k of the electron wave vector. The dashed line shows the corresponding intensity variation (the Gabor zone plate) from an s-wave scatterer.

If the artificial s-wave scatterer above is replaced by a Cu atom scatterer placed at the same distance from the emitter, the resulting variation of $I(k_z)$ with k_z may be evaluated from (23), with $f(k_z/k)$ evaluated from (9) with calculated Cu atom phase shifts δ_l. This variation is illustrated by the solid curve in Fig. 1, over the same range of k_z/k. Several important differences from the case of the s-wave scatterer are noted. First, a very narrow region around $k_z/k=1$ contains an extremely intense peak, due to the forward bias of the atomic scattering factor. Second, it will be noticed that the oscillation frequency of $I(k_z)$ with k_z is distinctly greater than that of the s-wave scatterer near the forward-scattering region around $k_z/k=1$ than for smaller values of this quantity, when the oscillation frequency approaches that of the dashed curve in Fig. 1. We can see that the value of $k_z/k\simeq 0.76$ corresponding to about 40° from the forward-scattering direction, and which is marked by the vertical dashed line, may be regarded as an approximate dividing line between these two regions. The Fourier

transform (20) applied to the region to the right of the vertical dashed line in Fig. 1, would therefore tend to peak at a "frequency" z somewhat greater than z_j, while that of the region to the left of that line would tend to peak around the true atom position. Notice, however, that since the amplitude of the oscillations is greater around the forward-scattering direction, the radial image function will tend to be dominated by a peak at $z > z_j$. Also, since $I(k_z)$ can be Fourier analyzed into sinusoidal functions of many different frequencies, each of which spans exactly the same range of k_z as in the case of the s-wave scatterer, it is inevitable that the reconstructed "image resolution" in this case will be poorer than the latter case. This could be regarded as a proof that the s-wave scatterer must give rise to the best-resolved reconstructed "image."

In an earlier paper[17] we have termed the full diffraction pattern from the s-wave source and s-wave scatterer a Gabor zone plate,[27] and that from the single atom scatterer an atomic zone plate. In that paper we calculated the RIF's in the directions joining source and scatterer for the two cases considered above, from the full diffraction patterns, using Barton's two-dimensional reconstruction algorithm (16). All the features of those RIF's are understandable in terms of the one-dimensional Fourier analysis above.

V. THE FORM OF THE SWIFT ALGORITHM FOR AUGER ELECTRON DIFFRACTION

In Barton's original formulation[8] of the Helmholtz-Kirchhoff reconstruction algorithm (16), he appealed to an approximate stationary-phase condition arising from the $e^{i\mathbf{k}\cdot\mathbf{r}_j}$ factor in the third term in an expression of the form (14) for the diffracted intensity to suggest that the reconstructed image intensity $|A(\mathbf{r})|^2$ would tend to peak at the atom position $\mathbf{r}_j$. We now know[16-18] that a much better stationary-phase condition results if the algorithm (16) is replaced by the scattered-wave included Fourier transform (SWIFT):

$$A(\mathbf{r})=\int \frac{I(\mathbf{k})}{K(\mathbf{k},\mathbf{r})} e^{-i\mathbf{k}\cdot\mathbf{r}} d\hat{\mathbf{k}} , \tag{26}$$

where we have termed $1/K(\mathbf{k},\mathbf{r})$ a scattered-wave kernel.[18]

To correct for the distorting effect of the source wave in Auger electron diffraction, we deduce, by replacing the quantities $\mathbf{r}_j$ in the angle-dependent parts of the coefficient of the term containing $e^{i\mathbf{k}\cdot\mathbf{r}_j}$ in (14) by the general vector $\mathbf{r}$, that the appropriate kernel is defined by

$$K(\mathbf{k},\mathbf{r})=\sum_l |A_l|^2 P_l(\hat{\mathbf{k}}\cdot\hat{\mathbf{r}})[f(\mathbf{k}\cdot\mathbf{r})]^* . \tag{27}$$

In view of the fact that this contains factors due to both initial and scattered wave, $1/K$ is perhaps best termed a source-and-scattered-wave kernel. Likewise, the SWIFT algorithm should in fact be regarded as a source-and-scattered-wave transform. Since in general K depends on both $\mathbf{k}$ and $\mathbf{r}$, the SWIFT algorithm is not of the form of a strict Fourier transform. As a result, the computational machinery of the fast Fourier transform cannot be used to evaluate (26), which to some minds tends to belie the acronym SWIFT.

If, however, the three-dimensional reconstructed image were built up from a sequence of RIF's, the SWIFT algorithm could indeed be implemented by a sequence of one-dimensional Fourier transforms. It is apparent from (21) that the SWIFT form of the algorithm for evaluating an RIF (20) in Auger electron diffraction is

$$A(z)=-k\int \frac{J(k_z)}{K_z(k_z)} e^{-ik_z z} dk_z , \tag{28}$$

where

$$K_z(k_z)=[f(k_z)]^* \sum_l |A_l|^2 P_l(k_z/k) , \tag{29}$$

which is independent of z. Since (28) is a true Fourier transform, K_z may be viewed as a deconvolution factor.

We show below that the view of the SWIFT algorithm as a deconvolution is both elegant and instructive. The diffraction pattern of a linear chain of Cu atom scatterers, separated from each other and from an s-wave source of electrons by the nearest-neighbor interatom distances of a Cu crystal was calculated by an exact multiple-scattering theory. Holographic RIF's along the Cu atom chain were reconstructed from this data by the one-dimensional form (20) of Barton's algorithm [Fig. 2(b)], and by the SWIFT algorithm (28) above, using the kernel $1/K_z$ [Fig. 2(c)]. Note that, although multiple scattering must be expected to be present in the case of the three-scatterer chain above, a kernel based on the kinematic plane-wave scattering factor is apparently able to achieve the desired result of returning the atom peaks to the positions of the atom centers. A comparison of these two plots with the Fourier transform

$$F(z)=\int [K_z(k_z)] e^{-ik_z z} dk_z \tag{30}$$

of the (inverse) scattered-wave kernel, shown in Fig. 2(a), is a graphic illustration of the deconvolution concept.

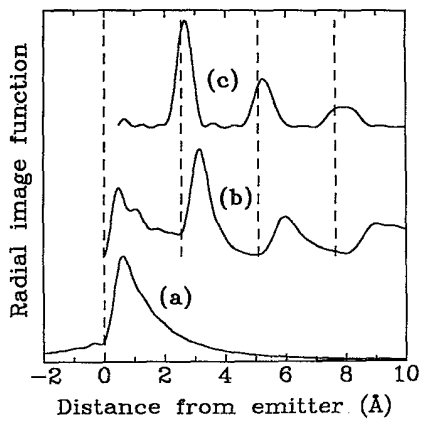

FIG. 2. Radial image function (RIF) reconstructed along the source-scatterer axis for the single Cu atom scatterer of Fig. 1 as calculated by Barton's Helmholtz-Kirchhoff integral (b); and our SWIFT algorithm (c). The corresponding Fourier transform of the deconvolution factor $K_z(k_z)$ is shown as (a). Curve (b) is seen to be the convolution of (c) with (a).

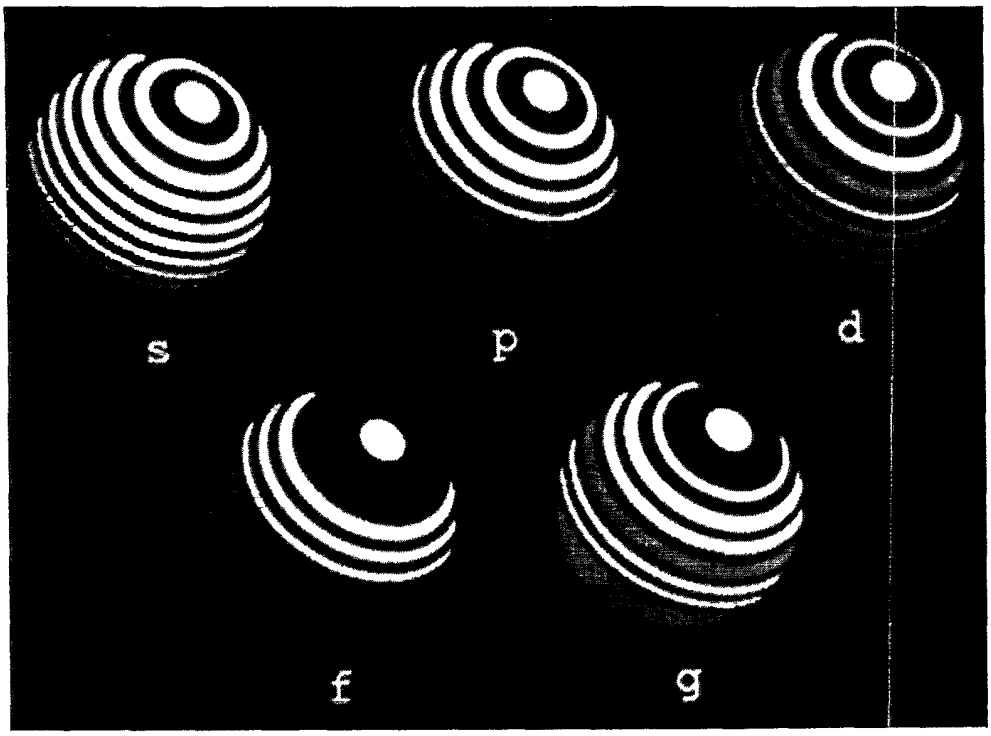

FIG. 3. Diffraction patterns due to off-axis Cu atom scatterers for emitted waves of s, p, d, f, and g angular momenta and other parameters as for Fig. 1.

VI. NON-s-WAVE EMITTERS

In Sec. II we pointed out that a single atom scatterer imposes the symmetry of the emitter-scatterer axis on the interference between an emitted and a scattered wave. On the usual model of Auger emission as occurring into incoherent sums of all the magnetic quantum number channels m of any particular angular-momentum channel l, the sum of the squared terms from the emitted wave is isotropic, and the sums of the squared terms from the scattered waves also possess azimuthal symmetry about the source-scatterer axis [see Eq. (14)]. Thus the diffraction pattern as a whole will have this azimuthal symmetry. A striking illustration of this is provided on Fig. 3, where emitted Auger electrons of 914-eV energy of single initial state angular momenta l ranging from 0 (an s wave) to 4 (a g wave) are assumed to be scattered by a single Cu atom 2.55 Å from the source at an angle of 45° to the diffraction pattern normal. The azimuthal symmetry referred to above is clearly seen.

In conjunction with our one-dimensional reconstruction algorithm (20), this symmetry enables us to analyze easily the effects on the reconstructed images of the angular momentum character of the reference wave. Taking the emitter-scatterer direction as the polar axis, we plot in Fig. 4 the intensity variations in Fig. 3 as functions of k_z/k. That for the s-wave emitter has already been plotted in Fig. 1. In that case, the Legendre polynomial $P_l(k_z)$ in (21) was a constant, and the deviation of the diffraction pattern from that of the ideal Gabor zone plate (dashed line in Fig. 1) is attributed solely to the dependence of the atomic scattering factor f of k_z, as manifested via the second (squared) term in curly brackets in (21), which acts to cause a rapid decay of $I(k_z)$ with decreasing k_z, and the third term (and its complex

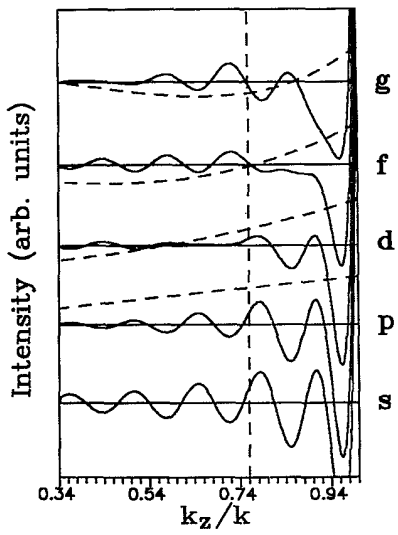

FIG. 4. Intensity variations of the diffraction patterns of Fig. 3 as functions of k_z/k, where the z axis is defined as the line joining source and scatterer. The angular momenta of the emitted waves are specified by the letters s–g in the usual spectroscopic notation.

conjugate) in which the variation of the phase σ, of f with k_z affects the periodicity of the oscillations of $I(k_z)$. As in the case of Fig. 1, we indicate by the vertical dashed line at $k_z/k=0.76$, the approximate dividing line between the parts of the curve oscillating at about the same frequency of the corresponding Gabor zone plate and that, close to the forward-scattering direction for which this frequency is higher.

For emitted waves with $l\neq 0$, $P_l(k_z)$ is no longer constant and this affects the form of $I(k_z)$. The variations of $I(k_z)$ with k_z for p ($l=1$), d ($l=2$), f ($l=3$), and g ($l=4$) wave emitters are also shown as solid lines in Fig. 4. Also plotted as dashed lines on the same graphs are the corresponding functions $P_l(k_z)$. Note that the plots of $I(k_z)$ against k_z for all the non-s-wave emitters are a result of multiplying the curve for the s-wave emitter with the Legendre polynomials, represented by the corresponding dashed lines. These Legendre polynomials have nodes which progressively approach the axis $k_z/k=1$ as the angular momentum quantum number l increases. The main effect on the corresponding plots of $I(k_z)$ is that the intensities in the regions around these nodes are severely reduced. In the cases of the p- and d-wave emitters, the first nodes of the corresponding Legendre polynomials fall well to the left of the vertical dashed line in Fig. 4, and thus do not significantly affect the high-intensity fringes to the right of the vertical dashed line. In the cases of the f- and g-wave emitters, on the other hand, the first bright finge next to the forward-scattering peak is completely suppressed.

These facts strongly influence the corresponding RIF's, which were calculated from (21) and (20) and displayed in Fig. 5. The image peak associated with the scattering atom is displaced substantially away from the scatterer for the s-, p-, and d-wave emitters, thereby giving rise to erroneous estimates of the atom position, unless a SWIFT algorithm is used, as discussed in Sec. V. The f- and g-wave emitters, however, reconstruct image peaks fairly well centered at the atom position, even with the use of Barton's reconstruction algorithm (16).

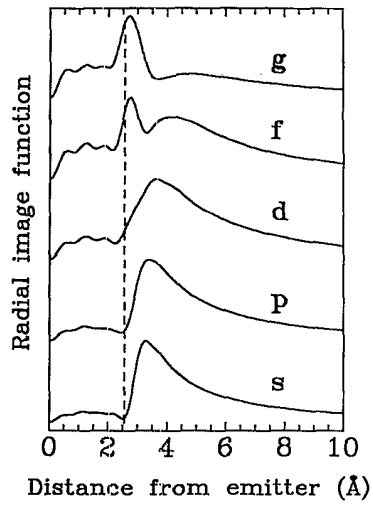

FIG. 5. Radial image functions along the source-scatterer axes, reconstructed by Barton's algorithm from the diffraction patterns of Fig. 3. The angular momenta of the emitted waves are specified as in Fig. 4.

The dependence of the diffraction intensities on k_z, as shown in Fig. 4, presents us a clear way to understand these results. It will be recalled that in our discussion of Fig. 1 in Sec. IV we pointed out that, in the case of an s-wave emitter and an atomic scatterer, the part of the $I(k_z/k)$ curve to the right of the vertical dashed line has a higher oscillation frequency than that of the ideal Gabor zone plate, while that to the left of that line approximated that frequency quite well. The distortion of the holographic image of the atom was thus seen to be largely due to the few large-intensity, higher-frequency fringes within about a 30° polar angle from the forward-scattering direction. These fringes survive, largely intact, in the cases of the s-, p-, and d-wave emitters. For the f- and g-wave emitters, however, Figs. 3 and 4 indicate most clearly that these distorting fringes are removed from the diffraction pattern by the first node of the Legendre function next to the forward-scattering direction. This leaves the fringes further away to correctly reconstruct the atom position, if the simple Fourier transform algorithm (16) or (20) were used.

VII. THE ANGULAR MOMENTUM OF 914-eV Cu L_3VV AUGER ELECTRON

The last section has drawn attention to the substantial effect on a holographic reconstruction of the angular-momentum character of the reference wave. None of the numerical reconstructions of holographic images to date have explicitly taken account of possible deviations of the reference wave from isotropy.[28] We emphasize here the importance of doing so by first drawing attention to the strong evidence that, contrary to the assumptions made in earlier calculations[29] of diffraction patterns from the Cu(100) surface due to the same Auger line, the angular-momentum state of the electron emitted by the well-known Cu L_3VV transition at 914 eV is not an s wave.

First, we review the evidence from calculations of the Auger matrix elements for this transition. If l_i represents the angular-momentum quantum number of the initial core hole, and l_j and l_k represent those of the final-state holes, Weissmann and Müller[14] have pointed out that the possible values of the angular momentum l of the emitted electron are determined by the relations

$$||l_i-|l_j-l_k||\leq l\leq l_j+l_k+l_i\ , \tag{31}$$

and

$$l_j+l_i+l_k+l=\text{even}\ . \tag{32}$$

When all three holes are atomic core states, (31) and (32) are easily applied to determine the possible angular momenta of the emitted electron. In the case of the Cu L_3VV transition, $l_i=1$ and l_j and l_k are determined largely by the dominant angular momentum of the local density of states (LDOS) of the valence band centered on Cu atoms. Since this LDOS is dominated by the Cu d band, we assume $l_j=l_k=2$. Substituting these values in

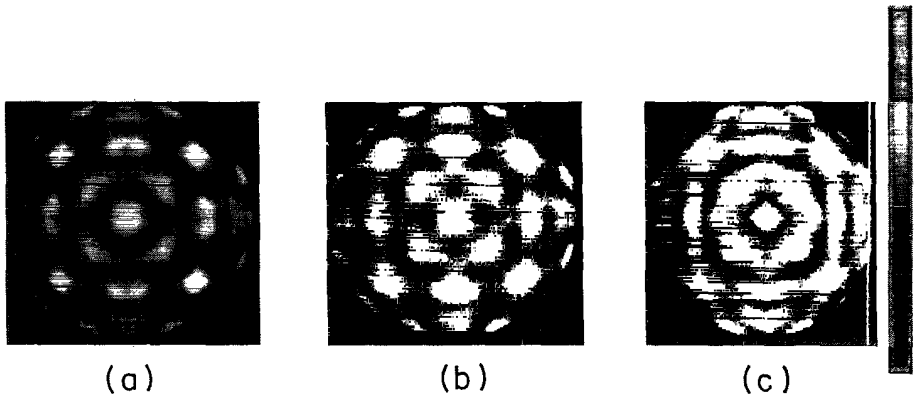

FIG. 6. Diffraction patterns due to 914-eV LVV Cu Auger electron emission from a Cu(100) surface: (c) represents the experimental diffraction pattern; (a) the computer simulation for an s-wave emitter; and (b) that for an f-wave emitter.

(31) and (32) it may be concluded that

$$l=1,\ 3,\ \text{or}\ 5\ . \tag{33}$$

Although of a much lower energy, the Cu $M_{2,3}VV$ Auger line at 62 eV involves core holes of the same angular momenta, and thus the same possible values of l. By comparing model calculations of line profiles of a diffraction pattern due to this Auger transition from a Cu(100) surface, Davis[30] found that the experimental data was fitted best for $l=3$. The LDOS on the atomic sites in Ni is expected to be likewise dominated by the d band, and calculations of the Auger matrix elements for the Ni $M_{2,3}VV$ transition by Aberdam *et al.*,[31] based on the theory of Asaad[32] have also concluded that, of the possible values (33) allowed by the selection rules, the transitions to the $l=3$ state were overwhelmingly the most likely. From these results it would appear probable that the electron emitted by the Cu L_3VV transition is likewise dominated by the angular momentum $l=3$.

We are able to test this hypothesis independently by comparing an experimental diffraction pattern from a Cu(100) surface with model calculations for initial emission states of differing values of l. The simulated patterns were calculated by evaluating the multiple scattering of electrons by a cluster of atoms surrounding inequivalent emitters in each of the outermost five layers of atoms on the surface. The cluster is divided into a set of concentric shells surrounding the emitter, and the intrashell and intershell scattering computed separately. This classification of the multiple-scattering paths enables considerable savings of computer time since it allows a

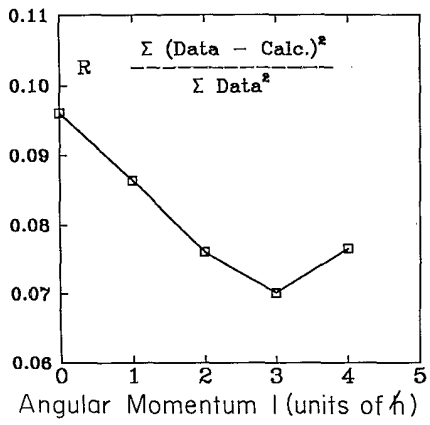

FIG. 7. Variation of the x-ray reliability factor (R) comparing the experimental diffraction pattern of Fig. 6(c) with computer simulations for emitted states of angular momenta, $l=0,1,\ldots,4$.

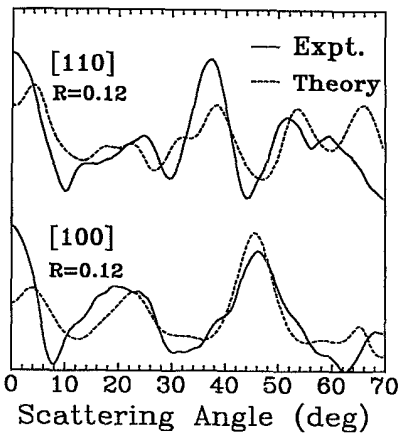

FIG. 8. Comparisons of the polar-angle variation of the experimental diffraction intensities of Fig. 6(c) along the [100] and [110] azimuths (solid lines) with those of the computer simulations for an s-wave emitter (dashed lines). The degree of agreement is monitored by the R factor, whose values are shown.

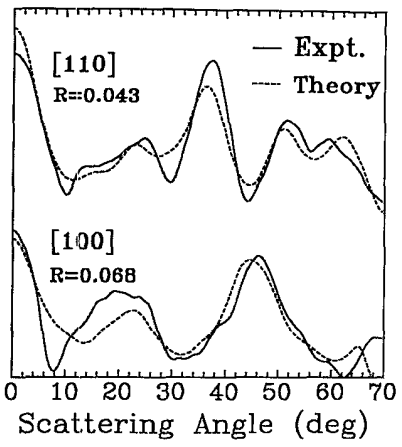

FIG. 9. Same as Fig. 8, except that the simulated profiles are due to an f-wave emitter. The substantially better agreement between experiment and theory compared with Fig. 8 can be seen by a visual comparison as well as from the significantly reduced R factors.

neglect of unimportant intrashell processes, while allowing a full treatment of the important forward multiple scattering. Further savings of computer time are achieved by exploitation of the point-group symmetry of the cluster of atoms surrounding the emitter. The final outgoing wave field is expressed as a linear combination of outgoing spherical waves centered on each emitter, and unlike all other existing methods of calculating Auger or photoelectron diffraction patterns, the multiple scattering does not need to be reevaluated for each data point on the diffraction pattern. The method of calculation bears a close similarity to one developed by Pendry and Saldin in the early 1980s for low energy electron diffraction (LEED).[33,34]

Figure 6(c) depicts an experimental Auger electron diffraction pattern from a Cu(100) surface, due to emission from the 914-eV L_3VV line. Figures 6(a) and 6(b) are diffraction patterns of the same energy, and calculated by the scheme described in the last paragraph, assuming Auger emission into states of $l=0$ and $l=3$, respectively. Visually, the pattern for $l=3$ appears to be in somewhat better agreement with the experimental data. In fact, we have simulated separate diffraction patterns for values l ranging from 0 to 4, and evaluated the degree of correlation between experiment and theory by means of the x-ray reliability factor

$$R=\frac{\sum_i (E_i-T_i)^2}{\sum_i E_i^2}, \tag{34}$$

where E_i and T_i represent the intensities of corresponding points on the diffraction patterns. The resulting plot R versus l is shown in Fig. 7, where the best correlation between experimental and theory is found for $l=3$.

This conclusion is underlined by Figs. 8 and 9, which compare polar angle profiles, along azimuths corresponding to some low-index crystallographic directions, of the intensities of the simulated diffraction patterns of s- and f-wave initial states, with those of the experimental data. The corresponding reliability factors are also shown in the same figures. Once again we see considerably better agreement for the f-wave ($l=3$) emitter.

The same is found when images reconstructed from these diffraction patterns by the algorithm (16) are compared. Figures 10(a), 10(b), and 10(c) show sections

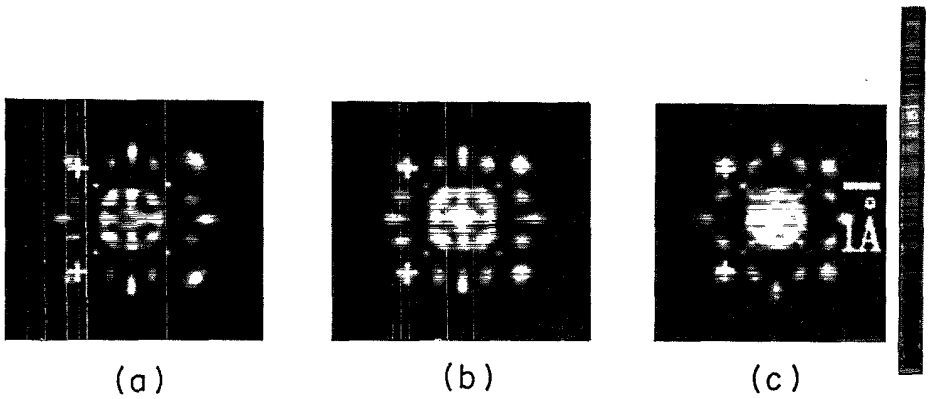

FIG. 10. Sections through the holographically reconstructed image (using Barton's algorithm) parallel to the crystal surface and passing through the plane of atoms immediately above an emitter atom: (a), (b), and (c) are calculated from the correspondingly marked diffraction patterns in Fig. 6. The positions of two of the nearest-neighbor atoms in this plane are marked by the crosses. Note that the image peaks associated with these atoms are almost coincident with these crosses on the reconstruction (c) from the experimental diffraction pattern and from the model of the f-wave emitter (b), but are somewhat displaced away from the crosses on that from the s-wave emitter model (a).

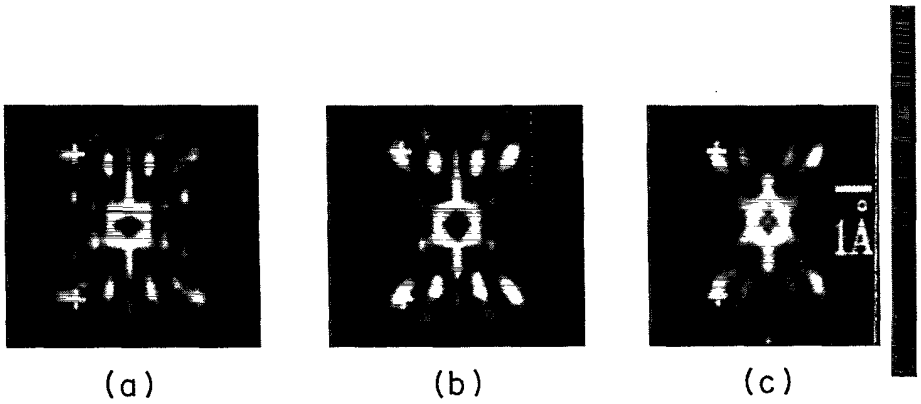

FIG. 11. Sections through the holographically reconstructed image (using Barton's algorithm) perpendicular to the crystal surface and passing through nearest-neighbor atoms to an emitter. Other details identical to Fig. 10.

through the resulting images parallel to the surface, and passing through four of the nearest-neighbor atoms, calculated from the diffraction patterns of Figs. 6(a), 6(b), and 6(c), respectively. Figures 11(a), 11(b), and 11(c) are the corresponding sections through the images, perpendicular to the surface and also passing through the known positions of nearest-neighbor atoms of a Cu crystal. In both of these figures, the reconstructed images from the simulated diffraction pattern of the f-wave emitter seem to be closer to that of the experimental

Perhaps most convincing are comparisons of the corresponding RIF's along a line joining an emitter and a nearest-neighbor scattering atom. Figure 12(a) compares the RIF calculated from the simulated data of the f-wave emitter with that from the experimental data, and Fig. 12(b) shows the corresponding comparison for that of the s-wave emitter. Not only is the peak on the RIF corresponding to the nearest-neighbor atom, but also all of the small radius peaks associated with artifacts due to the forward-scattering peaks of other scattering atoms are faithfully reproduced from the simulated diffraction pattern due to the f-wave emitter.

The detailed agreement between the experimental results and the f-wave calculations shown in Figs. 6–12, are among the best that have been achieved in work on forward-scattering diffraction patterns due to Auger, photoemission or Kikuchi sources. This gives us much confidence in the conclusion we draw that the 914-eV Cu L_3VV Auger transition emits an electron primarily into the $l=3$ angular-momentum channel. In the next section we will make use of this conclusion to implement an appropriate algorithm for correcting for the effect on the holographically reconstructed image from an experimental diffraction pattern from the above Auger line.

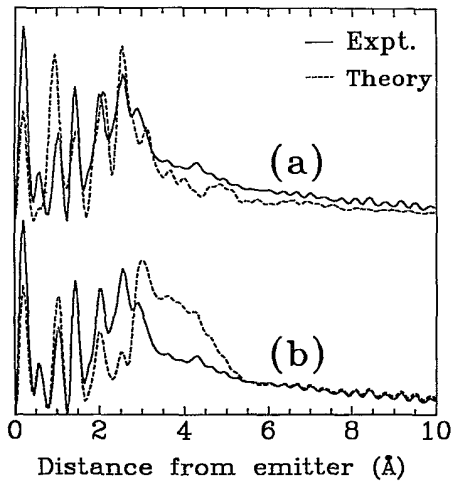

FIG. 12. Comparisons of radial image functions (RIF's) joining an emitter and a nearest-neighbor scatterer from the reconstructed images of which Figs. 10 and 11 represent sections. The RIF from the experimental diffraction pattern of Fig. 6(c) is represented by the solid lines. Separately compared with this are the RIF's from (a) the f-wave emitter model and (b) the s-wave emitter. Substantially better agreement is seen on (a), where the positions of all the peaks between source and scatterer are correctly reproduced.

VIII. CORRECTING FOR THE ANISOTROPY OF THE REFERENCE WAVE

We begin with a model calculation which illustrates the effect on an image reconstructed from a diffraction pattern due to an f-wave initial state and a single atom scatterer. We reproduce in Fig. 13(a) the RIF along the emitter-scatterer axis, calculated from Barton's reconstruction algorithm (16). As we pointed out in our discussion in Sec. VI, in this case a peak on the reconstructed image is correctly reproduced at the atom position.

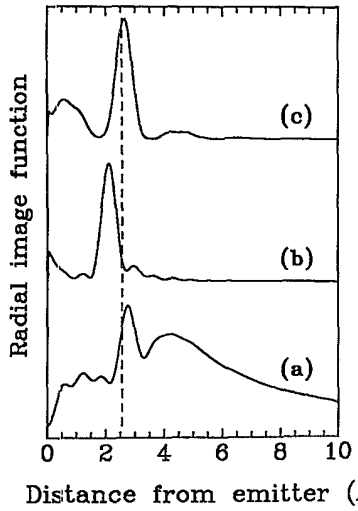

FIG. 13. Radial image functions from a diffraction pattern of the single Cu-atom scatterer and f-wave emitter (e.g., that marked f in Fig. 3): (a) was calculated by Barton's algorithm; (b) from a SWIFT algorithm containing only the atomic-scattering factor, and (c) a SWIFT algorithm which corrects also for the deviation of the source wave from s-wave character. Note that for the reasons noted in the discussion of Fig. 4, Barton's algorithm fortuitously reproduces the atom peak in (a) for the f-wave emitter, while the incomplete SWIFT algorithm moves the peak too close to the emitter in (b). However, the full SWIFT algorithm correctly reproduces the atom peak in (c).

One conclusion might then be that, in such a case, it is unnecessary to employ the SWIFT reconstruction scheme since the simpler Barton algorithm suffices in correctly reproducing atom images. Since, however, the SWIFT algorithm remains the theoretically correct one, it is interesting to examine its effect.

If, as in all numerical work to date, we were to include in the SWIFT kernel only the anisotropy of the atomic scattering factor, the kernel would take the form of just $1/[f(\mathbf{k}\cdot\mathbf{r})]^*$. Using this form of the kernel in the SWIFT algorithm (26) the RIF shown in Fig. 13(b) is obtained. The atom image appears displaced to a position *closer* to the emitter than the scattering atom. Thus if the SWIFT algorithm were implemented without proper account of the anisotropy of the reference wave, an image could be reconstructed which is actually *less accurate* than one from Barton's simpler algorithm.

However, on employing the correct form of the SWIFT kernel for this case, defined by

$$K(\mathbf{k},\mathbf{r})=P_3(\hat{k}\cdot\hat{r})[f(k\cdot r)]^* , \tag{35}$$

which properly accounts for the form of the reference wave, not only is the image peak once again correctly reproduced at the true atom position, but also the prominence of this peak relative to its background has been enhanced compared to the original RIF in Fig. 13(a).

We next examine the effects of the above two forms of SWIFT kernel on the reconstruction of images from the experimental Auger electron diffraction pattern of Fig. 6(c). At this point we recall that the SWIFT kernel (27) was derived assuming the presence of just a single scattering atom. In the presence of many simultaneous scatterers, to a first approximation the resulting diffraction pattern may be thought of as a combination of many overlapping zone-plate patterns like those of Fig. 4. Provided the central peak of such a zone plate does not dominate, this overlap has no great effect, and each individual zone plate may be regarded as the reproducer of the image of the scatterer which gave rise to it. This is the basis of the zone-plate model of optical holography, and indeed, also applies well for so-called backscattering diffraction patterns, e.g., one due to Auger emission from an adsorbate on a surface. In forward-scattering electron diffraction patterns of electron energies in excess of about 500 eV, e.g., the diffraction patterns of Fig. 6, however, the overwhelming dominance of the forward-scattering peak of a particular zone plate seriously perturbs the holographic reconstructing properties of other zone plates. Before the application of a reconstruction algorithm such as (16) or (26), therefore, it is important to reduce the effect of such forward-scattering peaks. A method of doing so has been proposed by Thevuthasan *et al.*,[35] which involves multiplying the diffraction intensities in the region of these peaks by Gaussian functions. This requires the identification on diffraction patterns of forward-scattering peaks. We have proposed an alternative method[36] which does not require this, and which is based on the idea of Fourier filtering. This technique eliminates from a diffraction pattern the low-frequency intensity variations associated with the spacings between forward-scattering peaks. We have shown that this suppresses the nonholographic low-radius peaks on RIF's Ref. (37) and leaves just the peaks associated with the atoms.

As a preliminary to a SWIFT deconvolution of the experimental Auger electron diffraction pattern of Fig. 6(c), we implemented this Fourier filtering procedure.[36] On subsequently performing an image reconstruction using Barton's algorithm (16), the RIF joining emitter and scatterer shown in Fig. 14(a) was obtained. As is the case of the model calculation for the f-wave emitter and the

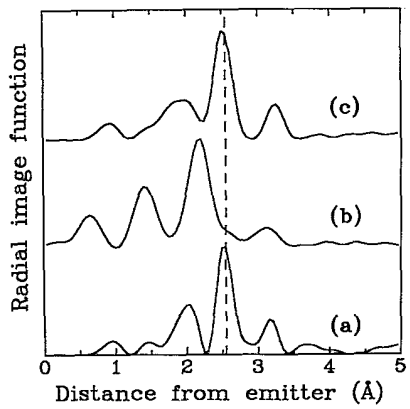

FIG. 14. Same as Fig. 13, but for RIF's joining a source and a nearest-neighbor scatterer, calculated from the experimental diffraction pattern of Fig. 6(c). The comments on Fig. 13 also apply here.

single atom scatterer shown in Fig. 13, the most prominent peak is found very close to the true atom position. We now recognize this as being due to the good fortune that the reference wave in this case is primarily of f angular-momentum character.

If the reconstruction were repeated by a SWIFT algorithm with a kernel containing just the atomic scattering factor f, as in the single scatterer case of Fig. 13, the reconstructed peak is moved closer to the emitter than the true atom position, as indicated in Fig. 14(b), and this incorrect SWIFT algorithm reproduces a worse image than Barton's algorithm (16). It is of interest to investigate the use of a SWIFT kernel of the form (35) even though this form was derived for a diffraction pattern from a single scatterer. The complication here is that the nodes of $P_3(\hat{\mathbf{k}}\cdot\hat{\mathbf{r}})$ in (35) will now give rise to singularities in the integrand of (26) since other scattering atoms will ensure that the corresponding values of $I(\mathbf{k})$ will not be zero. This problem may be overcome by first adding a small imaginary constant to the denominator in (35) and, second, by ensuring that the integrated diffraction intensity around the rings corresponding to the positions of the nodes of P_3 is zero. The latter can be done by subtracting the appropriate constant from the diffraction intensities I in (26). Application of the resulting algorithm to the Fourier filtered diffraction pattern of Fig. 8(a) gives rise to the RIF shown in Fig. 14(c), where the image peak is centered correctly at the atom position.

IX. DISCUSSION AND CONCLUSIONS

The importance of taking account of the anisotropy of the scattering factors of atoms in the computer reconstruction of the atomic structure around atomic emitters of electrons from diffraction patterns has been widely appreciated recently. We have pointed out in this paper the equal importance of taking account of the angular-momentum character of the reference wave.

We have demonstrated this with numerical calculations on model systems of Auger electron holography, by reconstructing atom images from diffraction patterns due to reference waves of different angular momentum. When a simple Helmholtz-Kirchhoff algorithm was used, the peaks associated with the atoms were found to reproduce the atom positions much better for f- and g-wave reference waves than those of lower angular momentum. We identify this as being due to the suppression of the large-intensity, high-frequency fringes near the forward-scattering direction, in the cases of these initial states by nodes of relevant angular-momentum states of the reference waves.

The advantages for accurate reconstruction of atomic positions of suppressing the intensities close to the forward-scattering directions have already been noticed by Thevuthasan *et al.*[35] Those workers achieved this by multiplying the diffraction intensities by an artificial (inverted) window function centered on the forward-scattering peaks. We have pointed out here that this very effect is accomplished incidentally by the very nature of the initial state in f- and g-wave Auger emission.

It is worthwhile here to point out that the approach has been taken by Tong and coworkers, in their small-window energy extension process[38,39] (SWEEP) is quite opposite to that of Thevuthasan *et al.* in that only the intensities very close ($\sim 30°$) to the forward-scattering directions are used as input to a reconstruction algorithm.

Our approach is to suppress neither the intensities close to the forward-scattering directions, nor those more than $\sim 30°$ from these directions, since information about all atoms is contained over the whole diffraction pattern (although the holographic fringes are much weaker away from the forward-scattering directions). We eliminate the distorting effects of the anisotropy of source and scattered waves over the whole of the diffraction pattern by the correct form of the source- and scattered-wave-included Fourier transform (SWIFT). This also has the effect of restoring the relative strengths of the more off-axis holographic fringes. The rationale for the small-window process, namely the elimination of the troublesome effects of other forward-scattering peaks, is achieved instead by our "Fourier filtering" procedure.[36] Our use of the information over the whole diffraction pattern should have the bonus of improving image resolution.

As a preliminary to demonstrating our algorithm in practice, we determine the angular-momentum character of the 914-eV L_3VV Auger emitted electron from Cu by comparing an experimental electron angular distribution from a Cu(100) surface with the results of model calculations for emitted electron states of different angular-momentum character. The calculations were performed by our scheme in which the clusters of scattering atoms around the emitters are subdivided into sets of concentric shells, thereby affording an efficient identification of the important multiple-scattering paths. The agreement found between the experimental data and the calculations for an f-wave emitter is excellent, and is monitored by the use of a reliability factor. The conclusion that the electrons of this particular Auger line are emitted primarily into an f-wave channel is in agreement with previous calculations of this particular Auger electron matrix element.

A SWIFT algorithm which correctly deconvolves the anisotropy of the atomic scattering factor *and* that of the reference wave is demonstrated with a model calculation for an f-wave emitter as well as with the experimental data of a Cu(100) Auger electron diffraction pattern.

ACKNOWLEDGMENTS

D.K.S. acknowledges support for this research by the donors of the Petroleum Research Fund, administered by the American Chemical Society. B.P.T. acknowledges support by a National Science Foundation Grant No. DMR-91-15987.

*Present address: IBM Almaden Research Center, 650 Harry Road, San Jose, CA 95120-6099.
[1]D. G. Frank, N. Batina, T. Golden, F. Lu, and A. T. Hubbard, Science **247**, 182 (1990).
[2]S. A. Chambers, Science **248**, 1129 (1990).
[3]W. F. Egelhoff, Jr., J. W. Gadzuk, C. J. Powell, and M. A. Van Hove, Science **248**, 1129 (1990).
[4]X. D. Wang, Z.-L. Han, B. P. Tonner, Y. Chen, and S. Y. Tong, Science **248**, 1129 (1990).
[5]D. P. Woodruff, Science **248**, 1131 (1990).
[6]L. J. Terminello and J. J. Barton, Science **251**, 1218 (1991).
[7]A. Szöke, in *Short Wavelength Coherent Radiation: Generation and Applications,* Monterey, CA, 1986, Proceedings of the Topical Meeting on Short Wavelength Coherent Radiation: Generation and Applications, edited by D. J. Attwood and J. Boker, AIP Conf. Proc. No. 147 (AIP, New York, 1986).
[8]J. J. Barton, Phys. Rev. Lett. **61**, 1356 (1988).
[9]D. K. Saldin and P. L. De Andres, Phys. Rev. Lett. **64**, 1270 (1990).
[10]G. R. Harp, D. K. Saldin, and B. P. Tonner, Phys. Rev. Lett. **65**, 1012 (1990).
[11]C. M. Wei, T. C. Zhao, and S. Y. Tong, Phys. Rev. Lett. **65**, 2278 (1990).
[12]G. R. Harp, D. K. Saldin, and B. P. Tonner, Phys. Rev. B **42**, 9199 (1990).
[13]W. Bambynek, R. W. Fink, H.-U. Freund, H. Mark, C. D. Swift, R. E. Price, and P. Venugopala Rao, Rev. Mod. Phys. **44**, 716 (1972).
[14]F. Weissmann and K. Müller, Surf. Sci. Rep. **105**, 251 (1981).
[15]S. Y. Tong, C. M. Wei, T. C. Zhao, H. Huang, and Hua Li, Phys. Rev. Lett. **66**, 60 (1991).
[16]S. Hardcastle, Z.-L. Han, G. R. Harp, J. Zhang, B. L. Chen, D. K. Saldin, and B. P. Tonner, Surf. Sci. **245**, L190 (1991).
[17]D. K. Saldin, G. R. Harp, B. L. Chen, and B. P. Tonner, Phys. Rev. B **44**, 2480 (1991).
[18]B. P. Tonner, Zhi-Lan Han, G. R. Harp, and D. K. Saldin, Phys. Rev. B **43**, 14 423 (1991).
[19]J. Korringa, Physica **13**, 392 (1947).
[20]W. Kohn and N. Rostoker, Phys. Rev. **94**, 1111 (1954).
[21]P. J. Durham, J. B. Pendry, and C. H. Hodges, Comput. Phys. Commun. **29**, 193 (1982).
[22]D. D. Vvedensky, D. K. Saldin, and J. B. Pendry, Comput. Phys. Commun. **40**, 421 (1986).
[23]H. C. Poon, D. Snider, and S. Y. Tong, Phys. Rev. B **33**, 2199 (1986).
[24]J. J. Rehr and R. C. Albers, Phys. Rev. B **41**, 8139 (1990).
[25]J. B. Pendry, *Low Energy Electron Diffraction* (Academic, London, 1974).
[26]V. Fritsche and P. Rennert, Phys. Status Solidi B **135**, 49 (1986).
[27]J. E. Kasper and S. A. Feller, *The Hologram Book* (Prentice-Hall, Englewood Cliffs, NJ, 1985).
[28]Although the incoherent sum over states characterized by different magnetic quantum numbers results in an apparently isotropic intensity distribution of the emitted wave in an Auger process, the *reference waves* of the holographic processes are the *individual magnetic quantum number states* which are *anisotropic* for all except *s*-wave emission.
[29]M.-L. Xu and M. A. Van Hove, Surf. Sci. **207**, 215 (1989).
[30]H. L. Davis, in Proceedings of the 7th International Vacuum Congress and 3rd International Conference on Solid Surfaces, Vienna, 1977, edited by R. Dobrozenski, F. Rüdenauer, F. P. Viehböck and A. Breth (Vienna, 1977), Vol. 3.
[31]D. Aberdam, R. Baudoing, E. Blanc, and C. Gaubert, Surf. Sci. **71**, 279 (1978).
[32]W. N. Asaad, Nucl. Phys. **44**, 415 (1963).
[33]J. B. Pendry, in *Determination of Surface Structure by LEED,* edited by P. M. Marcus and F. Jona (Plenum, New York, 1984), p. 3.
[34]D. K. Saldin and J. B. Pendry, Surf. Sci. **162**, 941 (1985).
[35]S. Thevuthasan, G. S. Herman, A. P. Kaduwela, R. S. Saiki, Y. J. Kim, W. Niemczura, M. Burger, and C. S. Fadley, Phys. Rev. Lett. **67**, 469 (1991).
[36]G. R. Harp, D. K. Saldin, X. Chen, Z. L. Han, and B. P. Tonner, J. Electron Spectrosc. Relat. Phenom. **57**, 331 (1991).
[37]Z.-L. Han, S. Hardcastle, G. R. Harp, H. Li, X.-D. Wang, J. Zhang, and B. P. Tonner, Surf. Sci. **258**, 313 (1991).
[38]S. Y. Tong, H. Huang, and Hua Li, in *Advances in Surface and Thin Film Diffraction,* edited by T. C. Huang, P. I. Cohen, and D. J. Eaglesham, M.R.S. Symposia Proceedings No. 208 (Materials Research Society, Pittsburgh, 1991).
[39]H. Huang, Hua Li, and S. Y. Tong, Phys. Rev. B **44**, 3240 (1991).